Figure S1

A

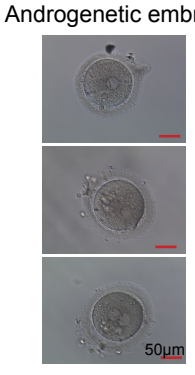

B

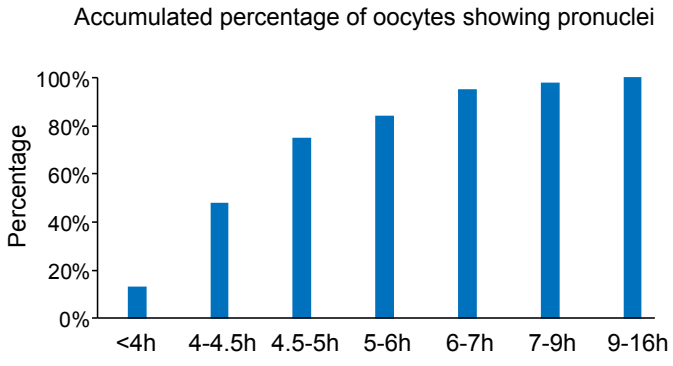

C

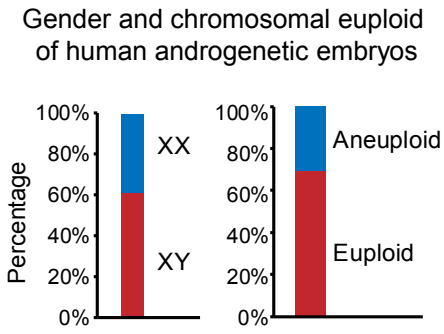

D

DNA fingerprint of genetic identification for donor gametes and diploid androgenic embryos

Androgenetic Diploid Embryo	Oocyte Donor 1	P-C Heritability* Freq(Donor1)	Oocyte Donor 2	P-C Heritability Freq(Donor2)	P-C Heritability Freq(Sperm)	Androgenetic (Yes/No)
31682-1	B31682	0.888055	B31682	0.888055	0.96616	Yes
30323-4	B30571	0.891004	B30323	0.891956	0.999767	Yes
31579-1	B31579	0.884245	B31579	0.884245	0.99989	Yes
31640-3	B31640	0.893617	B31640	0.893617	0.999864	Yes
30497-3	B30497	0.987566	B30497	0.987566	0.956267	NO
31572-2	B31572	0.931614	B31572	0.931614	0.999864	Yes
30400-1	B30400	0.898622	B30400	0.898622	0.999926	Yes
08822-1	B08822	0.889883	B08822	0.889883	0.999873	Yes
30931-3	B30931	0.891324	B30931	0.891324	0.99989	Yes
30931-2	B30931	0.921917	B30931	0.921917	0.985571	Yes
14822-1	B30931	0.879684	B14822	0.879912	0.999421	Yes
27250-1	B27250	0.856771	B27250	0.856771	0.999676	Yes
27250-2	B27250	0.858671	B27250	0.858671	0.99966	Yes
31578-1	B31578	0.992213	B31578	0.992213	0.96616	NO
31640-2	B31640	0.877962	B31640	0.877962	0.996998	Yes

E

Genome-wide copy number variation of human diploid blastocyst

Androgenetic Diploid Embryo	Copy number variation
31682#1	Arr [h19] 46,XX
30323-4	Arr [h19] 46,XX
31579-1	Arr [h19] 46,XY
31640-3	Arr [h19] 46,XY
31572-2	Arr [h19] 48,XY ， +2， +5
30400-1	Arr [h19] 46,XY
08822-1	Arr [h19] 46,XY ， del（1）(q41→q44)
30931-3	Arr [h19] 46,XY
30931-2	Arr [h19] 38,XY,-5,-6,-7,-13,-19,-20,-21
14822-1	Arr [h19] 46,XY,patialy UPD
27250#1	Arr [h19] 46,XX(upd)(Genome-wide UPD all chromosome)
27250#2	Arr [h19] 46,XX(upd)(Genome-wide UPD all chromosome)
31640-2	Arr [h19] 34,XX,-1,-3,-5,-10,-11,-13,-15,-16,-18,-20,-21,-22

Figure S1. Generation of human diploid parthenogenetic and AG embryos
A. Haploid AG embryos after removal of the female pronucleus. B. After ICSI, pronuclear formation of the biparental embryos. After ICSI for 5-6 h, the pronucleus appeared in more than 80% of the embryos. C. The rate of sex and chromosomal euploidy of human AG embryos. D. Genetic identification of the parental-child relationship for donor gametes and diploid embryos. E. The copy number variation of the human diploid AG embryos produced in our study

Figure S2

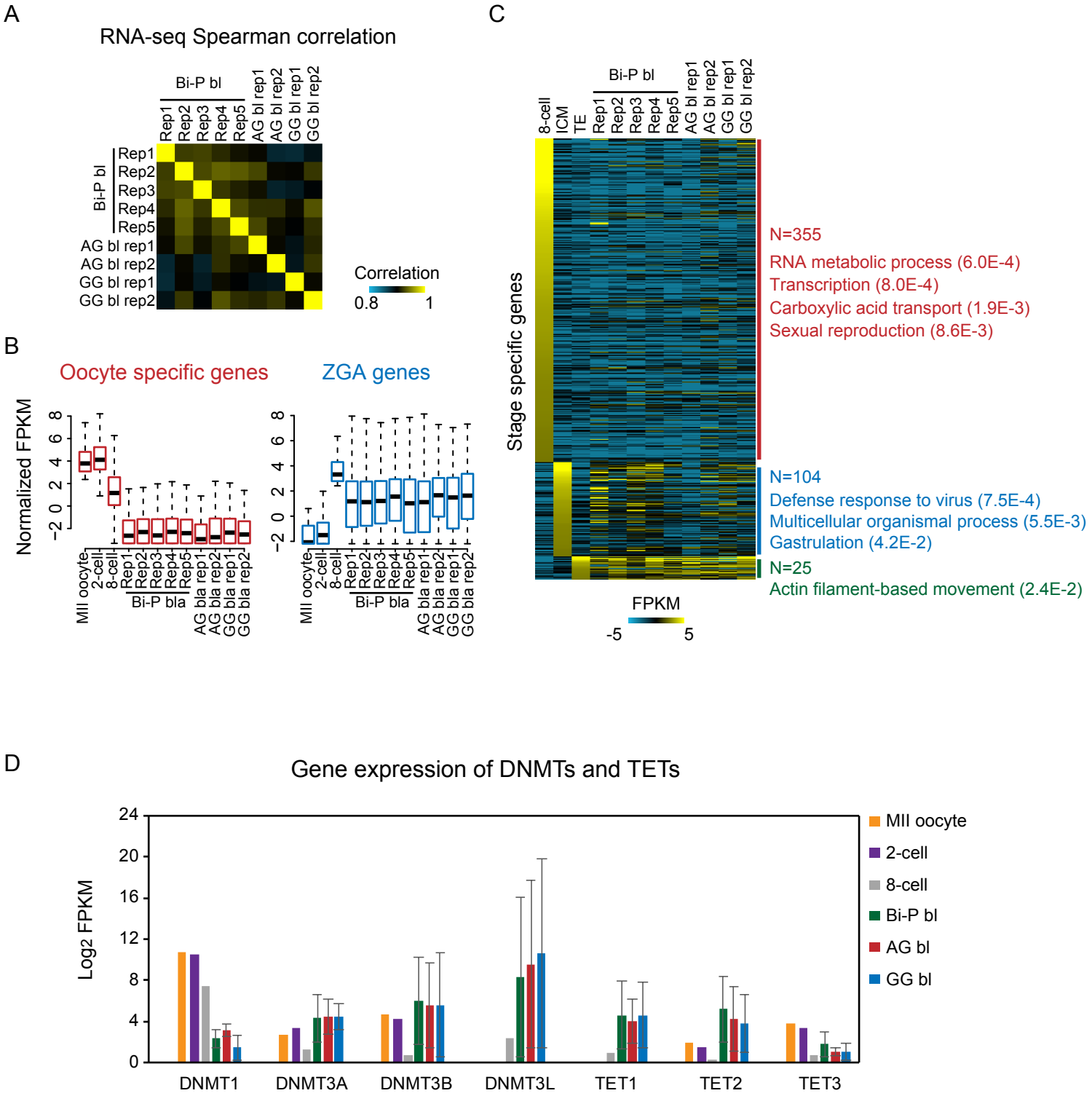

Figure S2. RNA-Seq analysis of human uniparental and Bi-P blastocysts

A. Spearman correlation of gene expression among AG, GG and Bi-P replicates. B. Oocyte specific and ZGA-related gene expression in MII oocyte, 2-cell, 8-cell, Bi-P, AG and GG blastocysts. C. Heatmap showing the expression of stage specific genes in 8-cell, ICM, TE, Bi-P, AG and GG blastocysts. The GO terms are also listed. For the identification of the stage-specifically expressed genes in the 8-cell, ICM and TE groups, the Shannon entropy-based method was used as previously described(Wu et al. 2018). Maternally expressed genes (FPKM≥1 in GV or MII oocytes) were first removed. For the remaining genes, only the genes with entropy scores less than 2 and FPKM greater than 10 in the expressed stage but not in other stages were selected as stage-specific genes. D. Gene expression of DNA methylation-related enzymes.

Figure S3

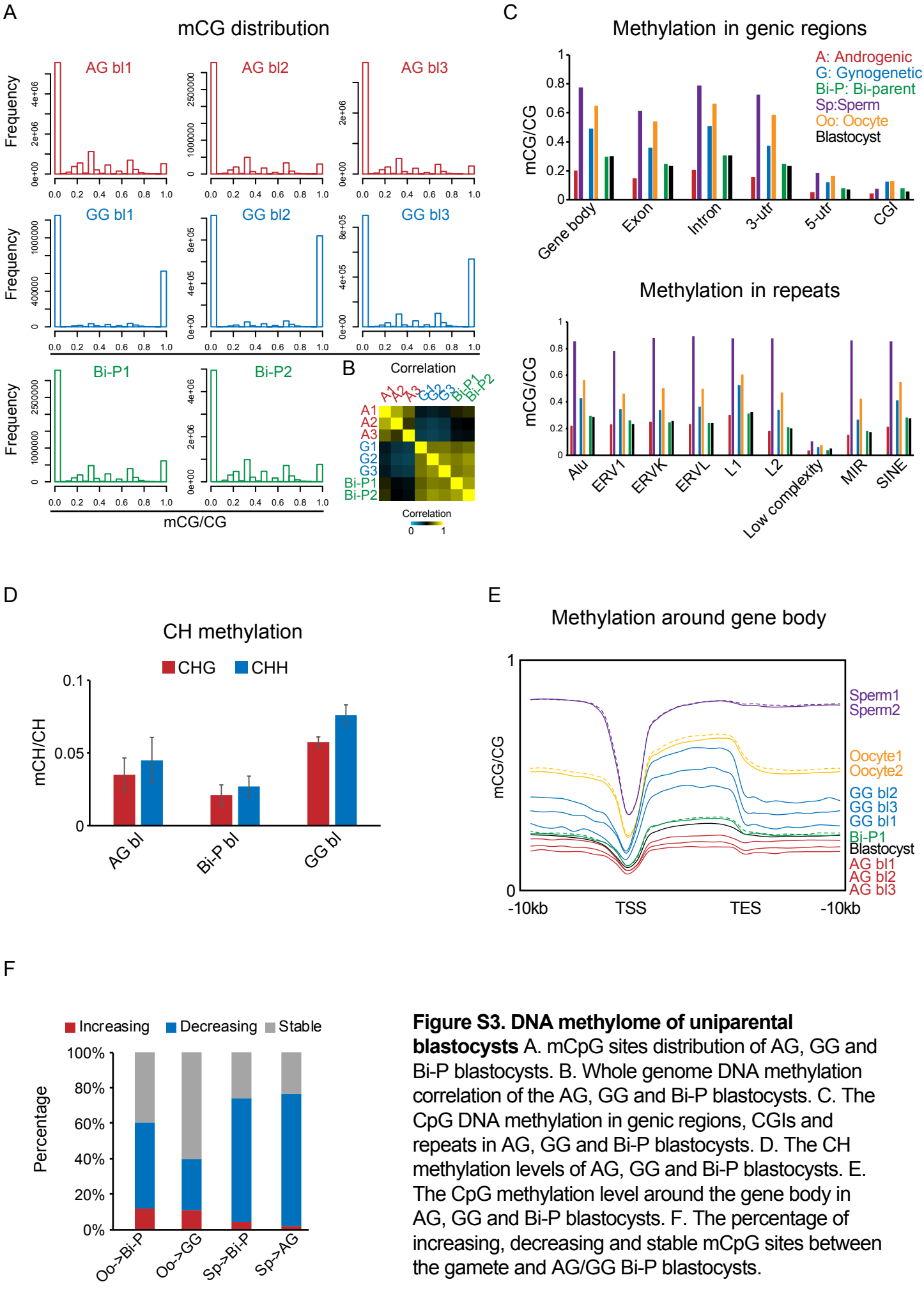

Figure S3. DNA methylome of uniparental blastocysts A. mCpG sites distribution of AG, GG and Bi-P blastocysts. B. Whole genome DNA methylation correlation of the AG, GG and Bi-P blastocysts. C. The CpG DNA methylation in genic regions, CGIs and repeats in AG, GG and Bi-P blastocysts. D. The CH methylation levels of AG, GG and Bi-P blastocysts. E. The CpG methylation level around the gene body in AG, GG and Bi-P blastocysts. F. The percentage of increasing, decreasing and stable mCpG sites between the gamete and AG/GG Bi-P blastocysts.

Figure S4

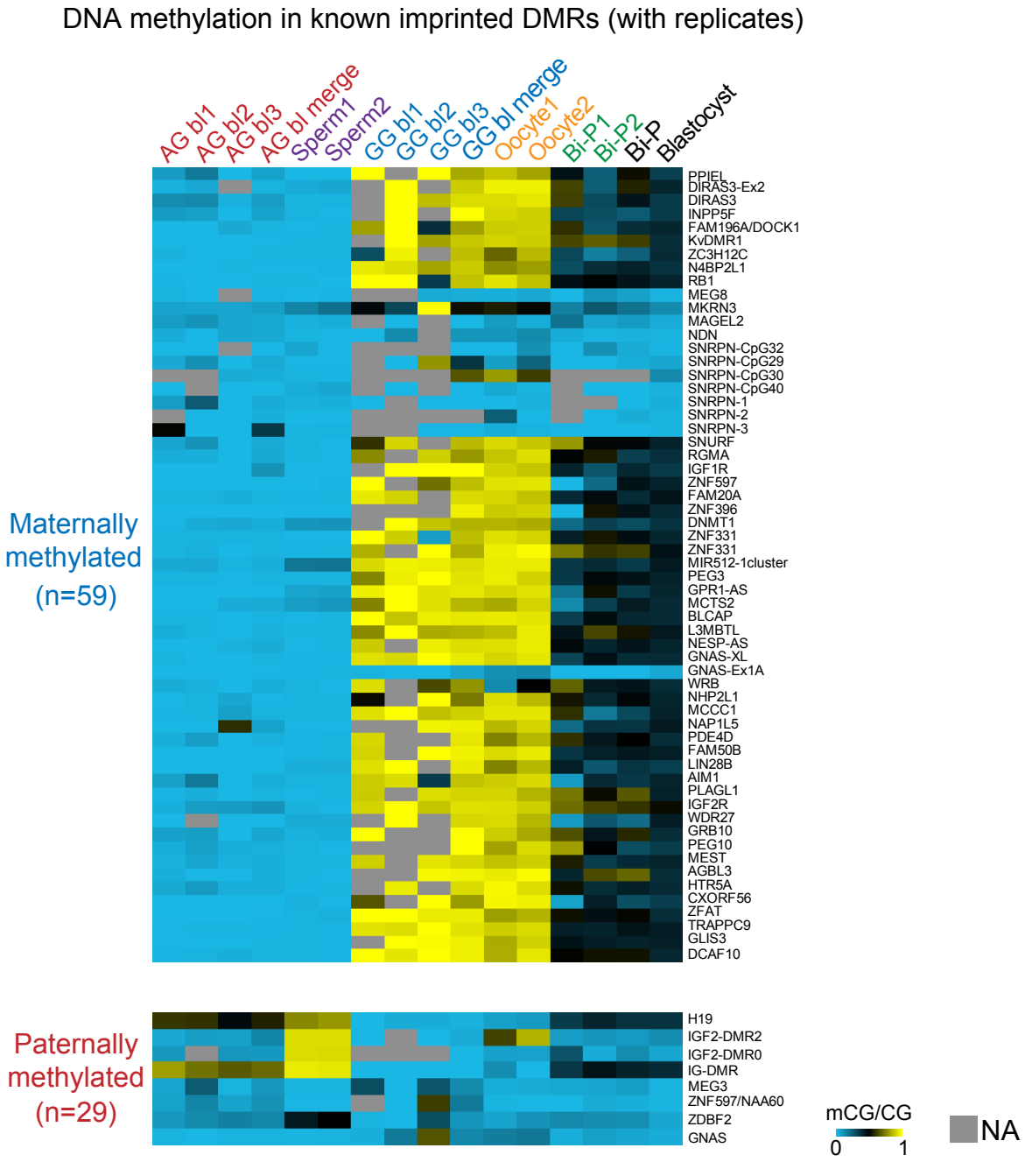

Figure S4. Heatmap of DNA methylation in known imprinted DMRs of each blastocyst
Heatmap showing the DNA methylation levels in known imprinted regions. Here, we showed the DNA methylation for each replicate in AG, GG, and Bi-P blastocysts for validation.

Figure S5

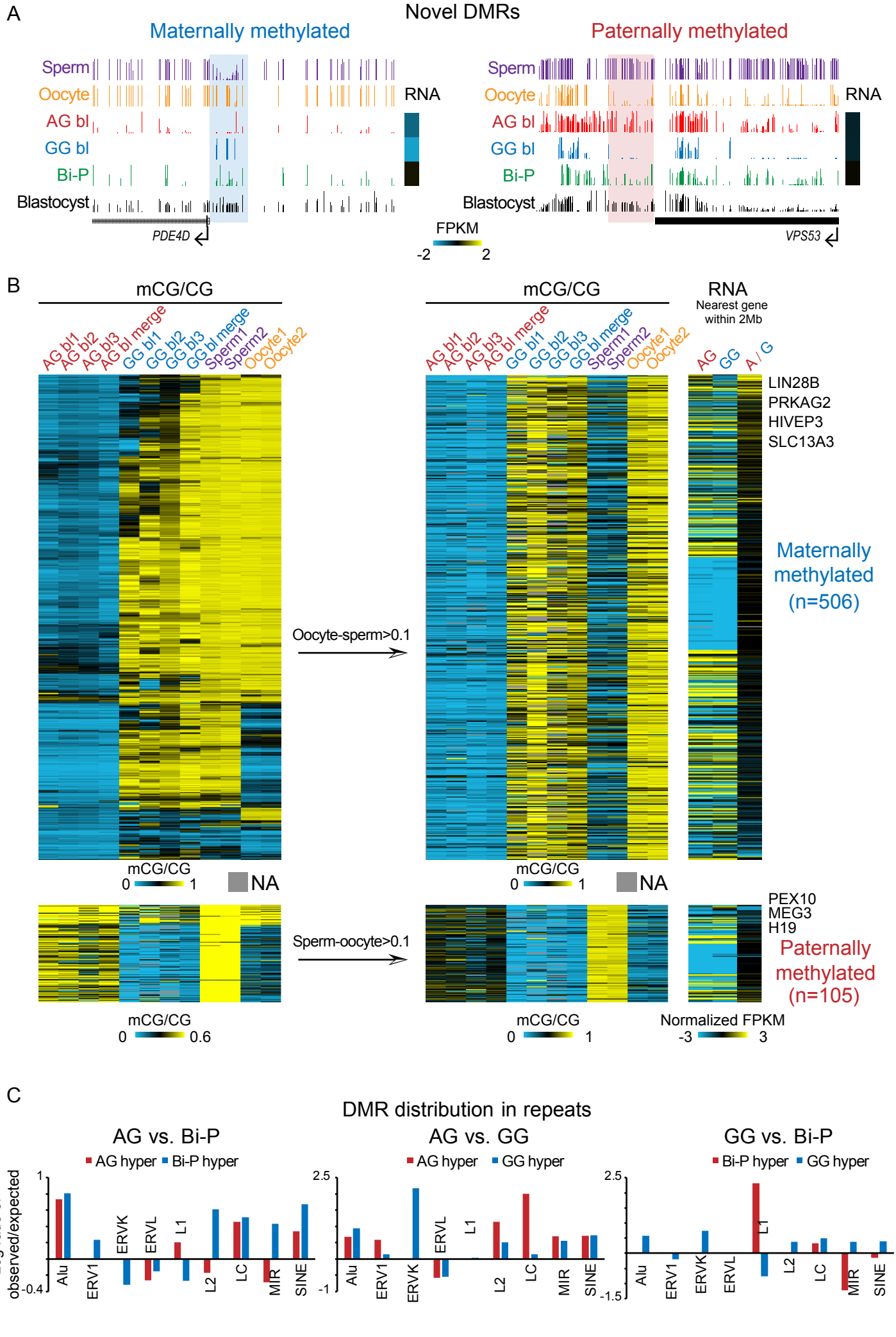
A
Novel DMRs
Maternally methylated
Paternally methylated
Sperm
Oocyte
AG bl
GG bl
Bi-P
Blastocyst
RNA
PDE4D
VPS53
FPKM
-2
2
B
mCG/CG
RNA
Nearest gene within 2Mb
AG bl1
AG bl2
AG bl3
AG bl merge
GG bl1
GG bl2
GG bl3
GG bl merge
Sperm1
Sperm2
Oocyte1
Oocyte2
AG
GG
A / G
LIN28B
PRKAG2
HIVEP3
SLC13A3
Maternally methylated (n=506)
Oocyte-sperm>0.1
mCG/CG
0
1
NA
PEX10
MEG3
H19
Paternally methylated (n=105)
Sperm-oocyte>0.1
0.6
Normalized FPKM
-3
3
C
DMR distribution in repeats
AG vs. Bi-P
AG hyper
Bi-P hyper
AG vs. GG
GG hyper
GG vs. Bi-P
Log ratio of observed/expected
Alu
ERV1
ERVK
ERVL
L1
L2
LC
MIR
SINE

Figure S5. Putative DNA methylation in DMRs

A. UCSC snapshot of putative maternal and paternal imprinted DMRs around PDE4D and VPS53. B. Heatmaps showing the DNA methylation levels for newly identified DMRs and the related gene expression. DNA methylation in 2, 4, and 8-cell embryos published previously was included as a control. The DMRs were firstly identified based on a pairwise comparison between AG and GG blastocysts as previously described (Zhang et al. 2018). Only those DMRs with changes in CG methylation levels between sperm and oocytes greater than 0.1 (for example, for maternal DMRs, the oocyte showed higher methylation levels than the sperm.) were taken as allelic putative DMRs. Here, the indicated genes are those nearest to the DMR in the 2 Mb region. C. The distribution of differential methylation regions (DMRs) in repeats.

Figure S6

A

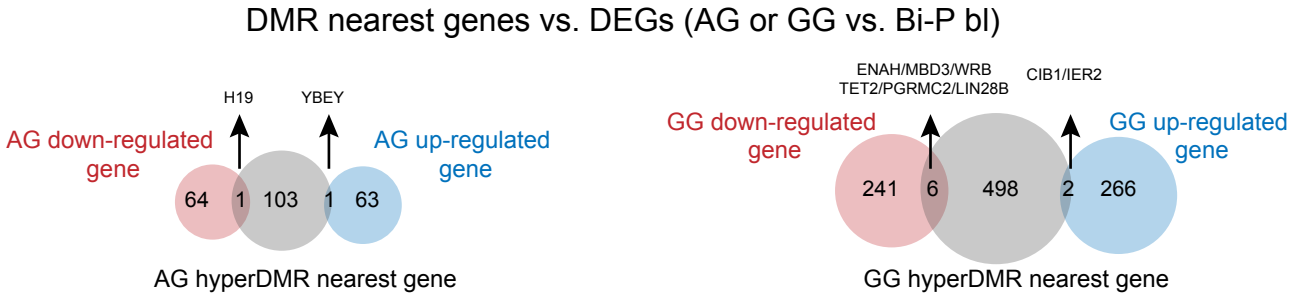

B

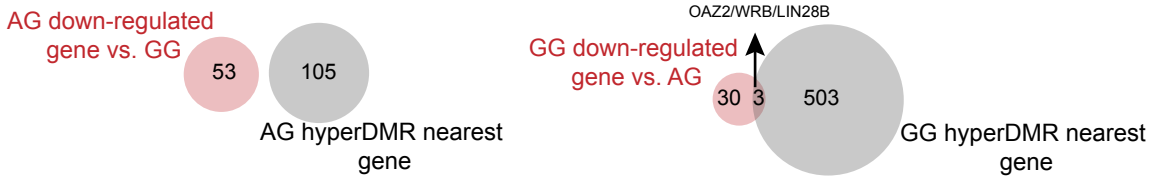

C

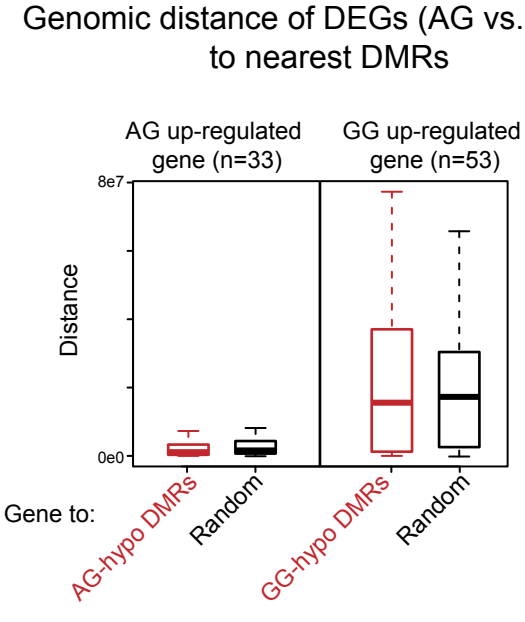

Figure S6. Relationship between novel identified DMRs and gene expression
A. DMRs between uniparental and Bi-P blastocysts overlapped with the DEGs. B. DMRs between the AG and GG blastocysts overlapped with the DEGs. C. Genomic distance of DEGs (AG vs. GG blastocysts) to DMRs. Random regions with the same length to each DMR were generated and used as controls.